Supplement of Earth Syst. Sci. Data, 14, 5463–5488, 2022
https://doi.org/10.5194/essd-14-5463-2022-supplement

Supplement of

A daily and 500 m coupled evapotranspiration and gross primary production product across China during 2000–2020

Shaoyang He et al.

Correspondence to: Yongqiang Zhang (zhangyq@igsnrr.ac.cn)

Supplement I: PML-V2 model description

The second generation of the Penman–Monteith–Leuning model (abbreviated as PML-V2) is a water–carbon coupled diagnostic biophysical model. Compared to the old version that does not calculate gross primary productivity (GPP) and the effect of CO_2 on evapotranspiration (ET), PML-V2 couples a photosynthesis model (Thornley, 1976) and an improved canopy stomatal conductance model (Yu et al., 2004) with the Penman–Monteith (PM) equation to estimate GPP and plant transpiration (E_c) collectively (Gan et al., 2018). Zhang et al. (2019) further improved PML-V2 by incorporating the vapor pressure deficit (VPD) constraint into GPP that is then used to constrain canopy conductance and E_c. Particularly, GPP is estimated by the gross assimilation rate integrated from leaf level to the canopy scale:

$$GPP = \int_0^{LAI} A_{g,VPD}\, dl\ , \tag{S1}$$

where l is the unit leaf area from top to full canopy, LAI is the leaf area index for the whole canopy, and $A_{g,VPD}$ is the gross assimilation rate at leaf level with the VPD constraint, calculated by the following two equations:

$$A_{g,VPD} = f_{VPD}\, A_g \tag{S2}$$

$$f_{VPD} = \begin{cases} 1, VPD \le D_{min} \\ \frac{D_{max}-VPD}{D_{max}-D_{min}}, D_{min} < VPD < D_{max} \\ 0, VPD \ge D_{max} \end{cases}\ , \tag{S3}$$

where $f(D_a)$ is the VPD constraint piecewise function, D_{min} is the minimum threshold when there's no vapor pressure constraint, D_{max} the maximum threshold when closing plant stomata leads to non-assimilation, and A_g is the gross assimilation rate at leaf level without the VPD constraint.

A_g is calculated by following Thornley (1976) as $\frac{A_m \beta I \eta C_a}{A_m \beta I + A_m \eta C_a + \beta I \eta C_a}$, where I is the flux density of photosynthetically active radiation (PAR), β is the initial slope of the light response curve to assimilation rate, and η is the initial slope of the CO_2 response curve to assimilation rate. A_m is the maximum photosynthetic rate obtained when both the flux density of PAR and C_a are saturated. Then, we can simplify Eq. S1 as Eq. S4.

$$GPP = f_{VPD} \frac{P_1 C_a}{k(P_2+P_4)} \left\{ kLAI + ln \frac{P_2+P_3+P_4}{P_2+P_3 \exp(kLAI)+P_4} \right\}, \tag{S4}$$

where $P_1 = A_m \beta I_0 \eta,\ P_2 = A_m \beta I_0,\ P_3 = A_m \eta C_a,\ P_4 = \beta I_0 \eta C_a$. I_0 is I at the top of the canopy, $k = k_Q$ is the extinction coefficient.

PML-V2 estimates G_c by integrating the stomatal conductance from the leave level into the canopy scale, as follows:

$$G_c = \int_0^{LAI} g_s\, dl\ , \tag{S5}$$

where g_s is the stomatal conductance at the leave-level. The g_s is calculated by an improved Ball model, as $m\frac{A_{g,VPD}}{C_a(1+VPD/D_0)}$ (Ball et al., 1987; Collatz et al., 1991; Yu et al., 2004), in which m is stomatal conductance coefficient, C_a is the atmospheric CO_2 concentration, D_0 is a parameter that represents the sensitivity of g_s response to VPD. So, G_c can be estimated as:

$$G_c = \frac{m\,GPP}{C_a(1+D_a/D_0)}, \quad \text{(S6)}$$

PML-V2 derives ET by separately estimating its three components, including E_c, evaporation from the soil (E_s), and canopy evaporation from precipitation interception (E_i), as follows:

$$ET = E_c + E_s + E_i, \quad \text{(S7)}$$

where E_c is calculated by P-M equation, given by:

$$E_c = \frac{\varepsilon A_c + (\rho c_p/\gamma) D_a G_a}{\varepsilon + 1 + G_a/G_c}, \quad \text{(S8)}$$

where G_c is a variable and couples with the photosynthesis process (Eq. S6); $\varepsilon = (de^*/dT)/\gamma$, in which de^*/dT is the curve slope relating saturation water vapor pressure to temperature and γ is psychrometric constant; the total available energy absorbed by surface is partitioned by leaf area index into canopy absorption (A_c), ρ is the air density; and $c_p$represents specific heat of air at constant pressure.

The ET component, E_s, depends on the soil water deficit and the soil absorbed energy flux, shown as:

$$E_s = \frac{f \varepsilon A_s}{\varepsilon + 1}, \quad \text{(S9)}$$

where A_s is the soil absorption and f is a unitless variable that is computed by a function of soil equilibrium evaporation and accumulated precipitation for each grid cell, given by:

$$f = \min\left(\frac{\sum_{i=1}^{N} P_i}{\sum_{i=1}^{N} E_{eq-s,i}}, 1\right), \quad \text{(S10)}$$

in which $E_{eq-s,i}$ is the average equilibrium evaporation rate at the soil surface for the ith day and P_i is precipitation for that day. Here the time-span for N can be set as 32 days since 16 to 32 days are reasonable (Morillas et al., 2013; Zhang et al., 2010). The component E_i is calculated by a modified rainfall interception model, Gash model, as shown in Eq. S11 (van Dijk and Bruijnzeel, 2001).

$$E_i = \begin{cases} f_v P, & P < Prcp_{wet} \\ f_v Prcp_{wet} + f_{ER}(P - Prcp_{wet}), & P \geq Prcp_{wet} \end{cases}, \quad \text{(S11)}$$

where f_V is the area ratio covered by intercepting leaves, f_{ER} is the ratio of average evaporation rate over average precipitation and assumes that it does not vary between the storms; P is daily precipitation; $Prcp_{wet}$ is the rainfall rate of the reference threshold if the vegetation canopy is wet.

References

Ball, J. T., Woodrow, I. E., and Berry, J. A.: A model predicting stomatal conductance and its contribution to the control of photosynthesis under different environmental conditions, in: Progress in photosynthesis research, Springer, 221–224, 1987.

Collatz, G. J., Ball, J. T., Grivet, C., and Berry, J. A.: Physiological and Environmental-Regulation of Stomatal Conductance, Photosynthesis and Transpiration - a Model That Includes a Laminar Boundary-Layer, Agric. For. Meteorol., 54, 107–136, https://doi.org/Doi 10.1016/0168-1923(91)90002-8, 1991.

van Dijk, A. I. J. M. and Bruijnzeel, L. A.: Modelling rainfall interception by vegetation of variable density using an adapted analytical model. Part 1. Model description, J. Hydrol., 247, 230–238, https://doi.org/10.1016/S0022-1694(01)00392-4, 2001.

Gan, R., Zhang, Y., Shi, H., Yang, Y., Eamus, D., Cheng, L., Chiew, F. H. S., and Yu, Q.: Use of satellite leaf area index estimating evapotranspiration and gross assimilation for Australian ecosystems, Ecohydrology, 11, e1974, https://doi.org/10.1002/eco.1974, 2018.

Morillas, L., Leuning, R., Villagarcia, L., Garcia, M., Serrano-Ortiz, P., and Domingo, F.: Improving evapotranspiration estimates in Mediterranean drylands: The role of soil evaporation, Water Resour. Res., 49, 6572–6586, https://doi.org/10.1002/wrcr.20468, 2013.

Thornley, J. H. M.: Mathematical models in plant physiology., Academic Press (Inc.) London, Ltd., 1976.

Yu, Q., Zhang, Y., Liu, Y., and Shi, P.: Simulation of the stomatal conductance of winter wheat in response to light, temperature and CO2 changes, Ann. Bot., 93, 435–441, 2004.

Zhang, Y., Leuning, R., Hutley, L. B., Beringer, J., McHugh, I., and Walker, J. P.: Using long-term water balances to parameterize surface conductances and calculate evaporation at 0.05° spatial resolution, Water Resour. Res., 46, W05512, https://doi.org/10.1029/2009wr008716, 2010.

Zhang, Y., Kong, D., Gan, R., Chiew, F. H. S., McVicar, T. R., Zhang, Q., and Yang, Y.: Coupled estimation of 500 m and 8-day resolution global evapotranspiration and gross primary production in 2002–2017, Remote Sens. Environ., 222, 165–182, https://doi.org/10.1016/j.rse.2018.12.031, 2019.

Table S1. The calibrated parameter values for nine PFTs used in PML-V2(China).

Parameter	ENF	EBF	MF	OSH	SAV	GRA	WET	CRO	BSV
β	0.0372	0.0389	0.0388	0.0289	0.0392	0.0499	0.0281	0.0391	0.0125
η	0.0429	0.0092	0.0223	0.0627	0.0151	0.0687	0.0312	0.0599	0.0416
m_s	3.7259	7.9996	7.7992	6.3180	6.3644	13.7067	21.8661	4.9718	5.5359
A_{m_25}	46.3662	9.6550	9.6552	12.8114	2.3992	6.8200	46.3697	29.9989	46.3572
Da	1.9870	0.9779	0.7992	0.8987	0.8828	0.5161	1.6043	1.9924	1.9952
k_Q	1.0000	0.5447	0.5058	0.5362	0.4231	0.9981	0.1054	0.2030	0.9954
k_A	0.6829	0.8002	0.8878	0.1426	0.8890	0.8972	0.8900	0.8856	0.6936
S_{sls}	0.1674	0.1155	0.0587	0.1598	0.0546	0.1276	0.0005	0.0091	0.1697
f_{ER}	0.0074	0.0156	0.0171	0.0696	0.1459	0.0031	0.0054	0.0106	0.1469
D_{min}	0.6503	0.6501	0.7307	0.7891	1.4103	1.4846	0.6517	1.3936	1.4895
D_{max}	5.3248	4.9345	5.4764	3.5021	6.4998	6.4721	5.5137	4.9973	6.4963

Table S2. Model performance for daily ET and GPP estimates at the 26 flux sites.

Site code	ET				GPP			
	NSE	RMSE (mm d^{-1})	R	Bias (%)	NSE	RMSE (g C m^{-2} d^{-1})	R	Bias (%)
ARCJZ	0.83	0.59	0.92	-13.39	0.87	1.03	0.94	17.66
BNXJL	0.42	0.72	0.65	-0.81	0.41	1.23	0.65	0.28
CF-CBF	0.82	0.49	0.91	-0.21	0.89	1.41	0.94	-2.26
CF-HBG_S01	0.81	0.57	0.91	-10.09	0.91	0.86	0.96	-10.52
CF-HBG_W01	0.78	0.73	0.90	-8.17	0.85	2.76	0.96	-12.26
CF-NMG	0.58	0.58	0.82	12.20	0.80	0.67	0.91	25.77
CF-QYF	0.70	0.71	0.85	-7.86	0.74	1.33	0.88	-2.55
CF-YCA	0.39	1.22	0.70	-18.05	0.60	4.59	0.82	-25.63
CN-Cng	0.70	0.65	0.85	-12.81	0.70	1.22	0.90	-28.22
CN-Du2	0.55	0.75	0.78	1.41	0.71	0.67	0.90	29.99
CN-HaM	0.81	0.45	0.94	19.01	0.78	1.42	0.92	-18.93
DMCJZ	0.84	0.77	0.94	-22.94	0.82	2.34	0.91	3.03
DSLZ	0.76	0.69	0.89	4.49	0.25	1.49	0.92	32.13
DXZ	0.41	0.90	0.79	-3.41	0.43	2.49	0.83	45.37
DYKGTSLZ	0.55	0.63	0.84	16.49	0.55	1.78	0.81	-16.85
GTZ	0.63	0.68	0.87	12.62	0.45	2.67	0.91	25.94
HLZ	0.65	0.74	0.87	7.96	0.82	2.66	0.92	-10.58
HZZHMZ	0.48	0.70	0.74	-27.03	0.41	0.33	0.74	-9.97
MYZ	0.74	0.61	0.92	12.47	0.29	2.39	0.91	60.83
QZ-BJ	0.68	0.70	0.84	-13.13	0.38	0.76	0.66	12.98
QZ-NAMORS	0.41	1.04	0.73	-27.81	0.44	0.60	0.67	-6.51
QZ-QOMS	0.05	0.50	0.69	39.42	0.64	0.26	0.80	-3.96
YJGRHG	0.36	0.39	0.67	-6.79	0.67	0.80	0.82	-3.03
YKGQLZZ	0.87	0.62	0.94	-15.74	0.85	2.48	0.92	-3.16
YKZ	0.39	0.77	0.74	-2.06	0.54	0.47	0.76	3.30
ZYSDZ	0.83	1.04	0.94	-2.68	0.77	1.77	0.91	29.44

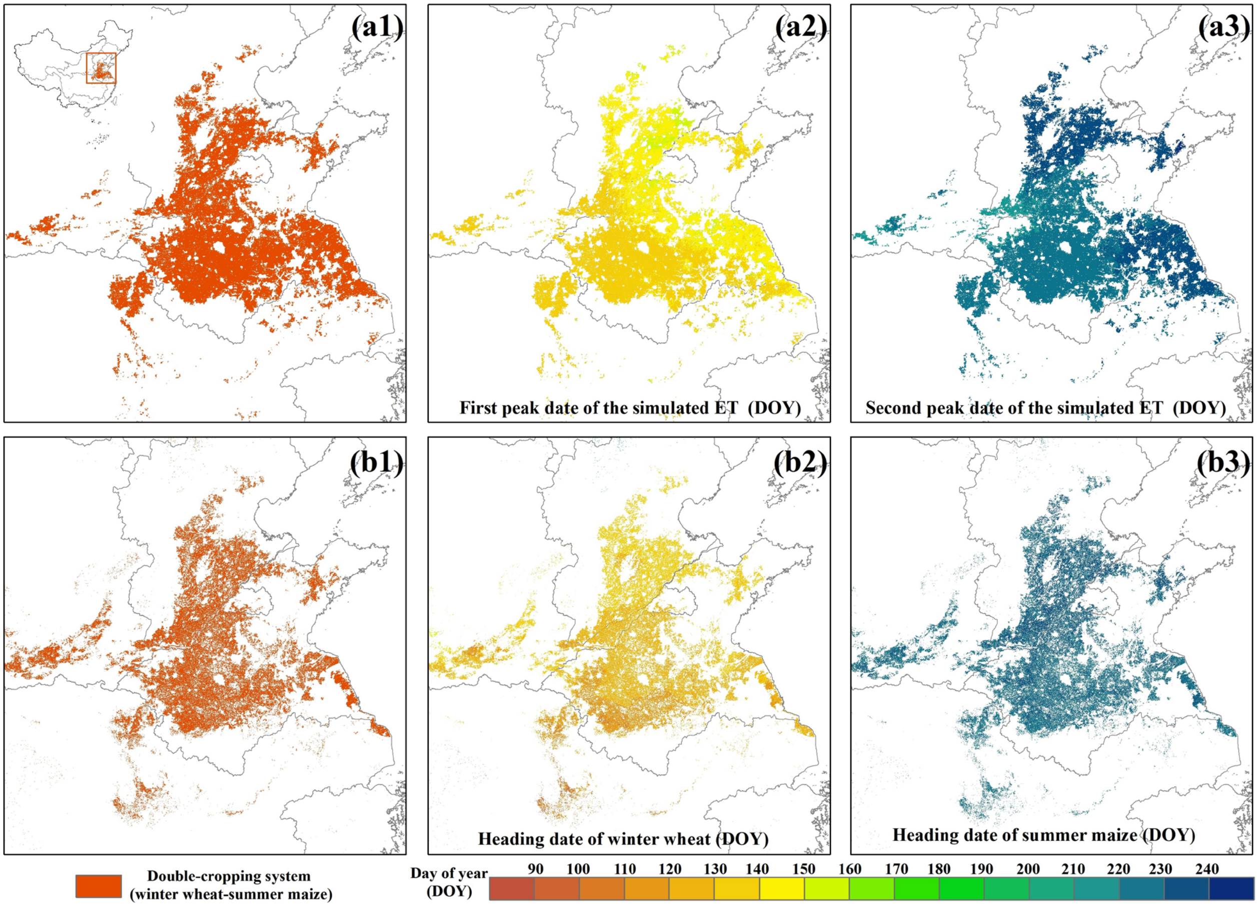

90 **Figure S1. Spatial patterns of the PML-V2(China) ET with double peaks in 2015 (a1) and the double-cropping croplands in 2015 from a crop phenological dataset (ChinaCropPhen1km) (b1); spatial patterns of the first peak dates (a2) and the second peak dates (a3) from the PML-V2(China) ET in 2015; and spatial patterns of the heading dates of winter wheat (b2) and those of summer maize (b3) from the crop phenological dataset in 2015.**